



Clinical correlates of R1 relaxometry and magnetic susceptibility changes in multiple sclerosis: a multi-parameter quantitative MRI study of brain iron and myelin

Giuseppe Pontillo^{1,2} · Maria Petracca³ · Serena Monti⁴ · Mario Quarantelli⁴ · Roberta Lanzillo³ · Teresa Costabile⁵ · Antonio Carotenuto³ · Fabio Tortora¹ · Andrea Elefante¹ · Vincenzo Brescia Morra³ · Arturo Brunetti¹ · Giuseppe Palma⁴ · Sirio Coccozza¹

Received: 4 December 2021 / Revised: 7 April 2022 / Accepted: 13 May 2022
© The Author(s) 2022

Abstract

Objectives The clinical impact of brain microstructural abnormalities in multiple sclerosis (MS) remains elusive. We aimed to characterize the topography of longitudinal relaxation rate (R1) and quantitative susceptibility (χ) changes, as indices of iron and myelin, together with brain atrophy, and to clarify their contribution to cognitive and motor disability in MS.

Methods In this cross-sectional study, voxel-based morphometry, and voxel-based quantification analyses of R1 and χ maps were conducted in gray matter (GM) and white matter (WM) of 117 MS patients and 53 healthy controls. Voxel-wise between-group differences were assessed with nonparametric permutation tests, while correlations between MRI metrics and clinical variables (global disability, cognitive and motor performance) were assessed both globally and voxel-wise within clusters emerging from the between-group comparisons.

Results MS patients showed widespread R1 decrease associated with more limited modifications of χ , with atrophy mainly involving deep GM, posterior and infratentorial regions ($p < 0.02$). While R1 and χ showed a parallel reduction in several WM tracts ($p < 0.001$), reduced GM R1 values ($p < 0.001$) were associated with decreased thalamic χ ($p < 0.001$) and small clusters of increased χ in the caudate nucleus and prefrontal cortex ($p < 0.02$). In addition to the atrophy, χ values in the cingulum and corona radiata correlated with global disability and motor performance, while focal demyelination correlated with cognitive performance ($p < 0.04$).

Conclusions We confirmed the presence of widespread R1 changes, involving both GM and WM, and atrophy in MS, with less extensive modifications of tissue χ . While atrophy and χ changes are related to global and motor disability, R1 changes are meaningful correlates of cognition.

Key Points

- Compared to healthy controls, multiple sclerosis patients showed R1 and χ changes suggestive of iron increase within the basal ganglia and reduced iron and myelin content within (subnuclei of) the thalamus.
- Thalamic volume and χ changes significantly predicted clinical disability, as well as pulvinar R1 and χ changes, independently from atrophy.
- Atrophy-independent R1 and χ changes, suggestive of thalamic iron and myelin depletion, may represent a sensitive marker of subclinical inflammation.

Keywords Multiple sclerosis · Magnetic resonance imaging · Atrophy · Quantitative susceptibility · Relaxometry

Giuseppe Pontillo and Maria Petracca share first authorship.

✉ Giuseppe Pontillo
giuseppe.pontillo@unina.it

¹ Department of Advanced Biomedical Sciences, University “Federico II”, Via Pansini 5, 80131 Naples, Italy

² Department of Electrical Engineering and Information Technology, University “Federico II”, Naples, Italy

³ Department of Neurosciences and Reproductive and Odontostomatological Sciences, University “Federico II”, Naples, Italy

⁴ Institute of Biostructure and Bioimaging, National Research Council, Naples, Italy

⁵ Multiple Sclerosis Centre, II Division of Neurology, Department of Clinical and Experimental Medicine, “Luigi Vanvitelli” University, Naples, Italy

Abbreviations

DD	Disease duration
EDSS	Expanded disability status scale
GM	Gray matter
HC	Healthy controls
MS	Multiple sclerosis
NAGM	Normal-appearing gray matter
NAWM	Normal-appearing white matter
QSM	Quantitative susceptibility mapping
T2-LL	T2 lesion load
TIV	Total intracranial volume
WM	White matter

Introduction

In multiple sclerosis (MS), the physiopathological mechanisms behind atrophy accrual and its impact on disability have been investigated and confirmed by several independent groups [1]. Nevertheless, the nature and clinical relevance of tissue microstructural abnormalities remain more elusive, partly because the coexistence of different pathological processes (demyelination, inflammation, axonal loss) represents a challenge for their characterization [2]. In recent years, semi-quantitative and quantitative MRI (qMR) methods have been developed to explore the nature of microstructural abnormalities, with a particular interest in MS being devoted to the assessment of iron and myelin, as these might offer a glimpse into the neurodegenerative process and tissue repair capability [3, 4]. Indeed, although iron accrual has to be interpreted with caution given the confounding effect of concomitant tissue loss [5, 6], iron depletion in white matter (WM) and in WM-rich structures such as the thalamus likely results from oligodendrocytes dysfunction and damage, with reduced myelination capacity and trophic support leading to neurodegeneration [7]. Among quantitative parameters, histological validation studies have confirmed the applicability of quantitative susceptibility mapping (QSM) for the assessment of iron content in the basal ganglia, where myelin intensities have almost no effect on susceptibility [8]. Within myelin-rich structures such as WM and thalamus, however, interpretation of susceptibility modifications is more challenging, as diamagnetic myelin and paramagnetic iron play opposite effects on susceptibility. In these regions, a susceptibility increase would be an expression of iron accrual/demyelination, while a susceptibility decrease would be an expression of iron depletion/increase in myelin content.

Another quantitative parameter, which more closely reflects tissue myelin content, is the longitudinal relaxation rate (R1). R1 is strongly associated with both myelin and axon content [9], but, according to postmortem analysis of brain tissue, it is primarily dependent on myelin content [10] and is among the most reliable myelin-sensitive MRI metrics [4].

Beyond the information that susceptibility and R1 changes (as proxies of iron and myelin content) can provide on the nature of microstructural abnormalities in MS, the clinical impact of such modifications remains unclear for several reasons. First, previous studies applying iron and myelin imaging in MS have mainly focused on global disability outcomes [11, 12] or have limited their investigation to selected regions of interest [13, 14]. Second, the fact that correlations with a disability might be driven by atrophy rather than modifications in iron and myelin per se has been rarely investigated [6]. Therefore, the goal of our work was to build on previous findings by exploring the impact of R1 and susceptibility changes on a wide range of disability outcomes (considering also manual dexterity and cognitive function), while accounting for atrophy, which is the main driver of disability accrual in MS [1] and, as recently highlighted, has a major impact on qMR measures [6, 15]. To this aim, we conducted a multi-parametric analysis of quantitative MR, together with brain volumetry, to (i) characterize the topographical distribution of atrophy, R1 and χ changes in the MS brain and (ii) clarify their impact on both cognitive and motor disability.

Materials and methods

Subjects

In this cross-sectional study, from February 2016 to January 2020, we prospectively enrolled MS patients diagnosed according to the 2010-McDonald criteria [16], along with age- and sex-comparable healthy controls (HC). Inclusion and exclusion criteria are shown in Fig. 1.

The study was conducted in compliance with ethical standards, approved by the local Ethics Committee and written informed consent was obtained from all subjects according to the Declaration of Helsinki.

Clinical and neuropsychological assessment

Within one week from the MRI, patients' clinical disability was quantified using the Expanded Disability Status Scale (EDSS) score [17], with disease course classified according to Lublin et al [18]. At the same time, patients were tested using the Symbol Digit Modalities Test (SDMT) [19] to assess cognitive processing speed, while ambulation and manual dexterity were probed through the Timed 25-Foot Walk (T25FW) and the 9-Hole Peg Test (9-HPT) [20], respectively. SDMT scores were expressed as Z-scores with reference to normative values in the healthy population, adjusting for age, gender, and education [19]. Similarly, T25FW and 9-HPT scores were referenced to normative values of an external population of MS patients [20] and averaged to obtain a single composite measure of motor performance. Z-scores were

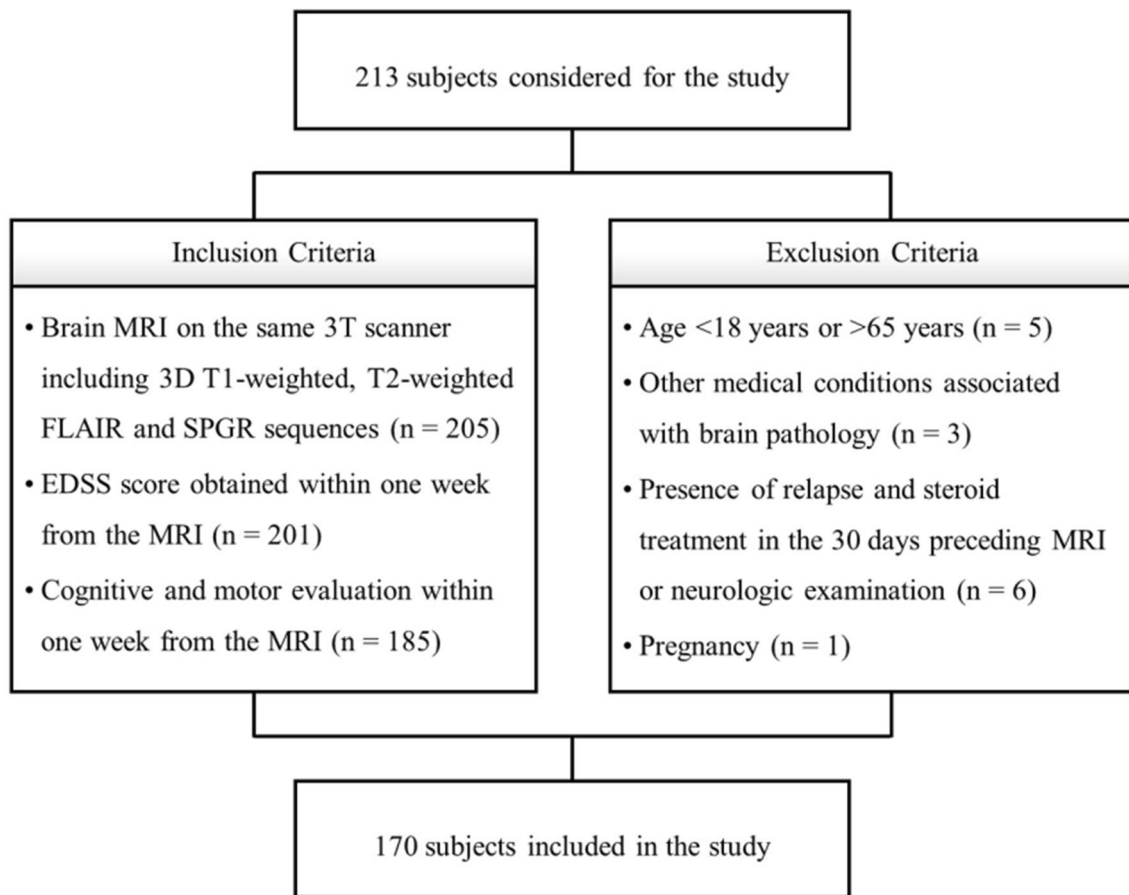


Fig. 1 Flowchart showing inclusion and exclusion criteria

flipped, as appropriate, to have higher scores always corresponding to better performances.

MRI data acquisition and preprocessing

All MRI exams were performed on the same 3T scanner (Magnetom Trio, Siemens Healthineers) and included a 3D T1-weighted sequence for volumetric analyses, a 3D T2-weighted FLAIR sequence for T2-hyperintense lesions detection, and lesion load (T2-LL) quantification and two spoiled gradient echo sequences for quantitative analyses [21]. Details about acquisition parameters and a thorough description of image preprocessing [22–24], including the computation of R1 and QSM maps [21, 25], are provided in the Supplementary Material, while a flowchart summarizing the main image processing and analysis steps is depicted in Fig. 2.

Briefly, quantitative maps were mapped onto the corresponding T1-weighted volumes, and demyelinating lesions were automatically segmented on FLAIR images via the Lesion Segmentation Tool (LST) toolbox (www.statistical-modelling.de/lst.html) and individual lesion probability maps

were used to fill lesions in T1-weighted images and binarized to compute T2-LL.

Subsequent processing steps were carried out following the voxel-based morphometry (VBM) [26] and voxel-based quantification (VBQ) [27] approaches: filled T1-weighted volumes were segmented into different tissue classes and normalized to a 1-mm isotropic template in MNI space via the standard pipeline implemented in the Computational Anatomy Toolbox (CAT12, <http://www.neuro.uni-jena.de/cat>), with the estimated spatial transformations also applied to quantitative maps. Finally, normalized GM and WM probability maps were modulated and smoothed using a 1mm full width at half maximum (FWHM) isotropic Gaussian kernel [28]. Instead, normalized R1 and χ maps were smoothed (1-mm FWHM isotropic Gaussian kernel) via the tissue-weighted smoothing procedure [27] implemented in the hMRI toolbox (<https://hmri-group.github.io/hMRI-toolbox>) to account for the partial volume contribution of tissue density in each voxel, resulting in tissue-specific smoothed quantitative maps in MNI space.

For each participant, total intracranial volume (TIV) was also estimated, and brain parenchymal, GM, and WM

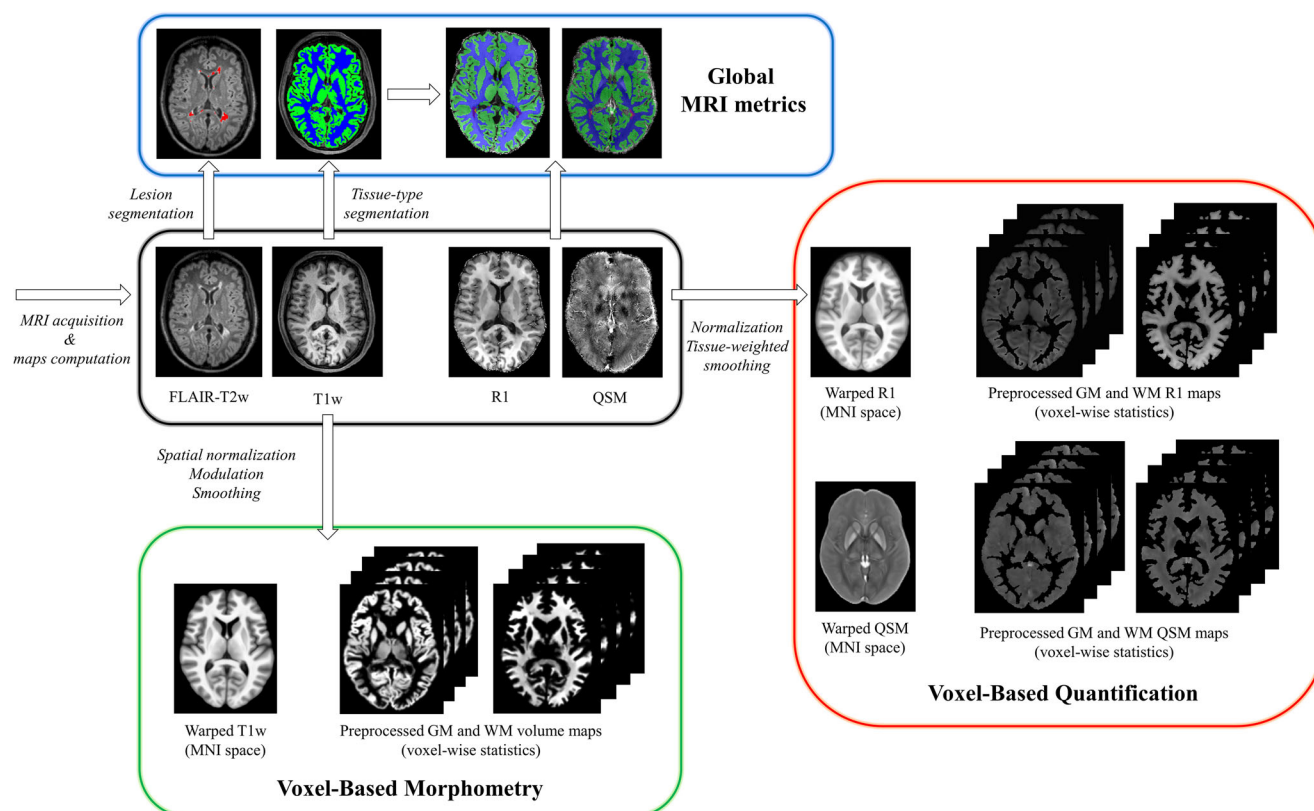


Fig. 2 Workflow illustrating the main image processing and analysis steps. Initially, quantitative maps were computed and mapped onto the corresponding T1-weighted volumes and demyelinating lesions were automatically segmented on FLAIR images. For voxel-based analyses, T1-weighted volumes were segmented into different tissue classes and normalized to a 1mm isotropic template in MNI space, with the estimated spatial transformations also applied to quantitative maps. Before entering

voxel-wise statistical analyses, normalized gray matter and white matter probability maps were modulated and smoothed, while normalized R1 and χ maps were smoothed via a tissue-weighted smoothing procedure to account for the partial volume contribution of tissue density in each voxel. Using lesion and tissue class masks, global brain volumes and median values of R1 and χ in normal-appearing tissues were also obtained

fractions (BPf, GMf, WMf) were computed. Additionally, individual normal-appearing GM and WM masks were obtained and used to extract median values of R1 and χ , while study-specific GM and WM masks were generated to restrict voxel-wise statistical comparisons in order to reduce possible spurious atrophy-related effects on VBQ analyses, as well as to ensure that each voxel was analyzed in only one subspace (i.e., GM or WM).

Statistical analysis

Unless otherwise specified, statistical analyses were carried out using the Statistical Package for Social Science (SPSSv25.0, IBM corp.) with a significance level $\alpha = 0.05$, and the Benjamini-Hochberg procedure was adopted for controlling the false discovery rate (FDR). Before running parametric analyses, assumptions of the linear model were preliminarily verified [29].

Between-group differences were tested with either Student *t* (age), Pearson chi-square (sex), or age- and

sex-corrected ANCOVA (tissue volumes and median R1 and χ values) tests.

As for the VBM and VBQ analyses, normalized, modulated, and smoothed tissue probability maps, as well as normalized and smoothed R1 and χ maps, were statistically analyzed, separately for GM and WM, to assess voxel-wise between-group differences using a nonparametric approach based on 5000 permutations applied to the general linear model [30] via the Threshold Free Cluster Enhancement (TFCE) toolbox (<http://www.neuro.uni-jena.de/tfce>). Age, sex, and TIV were included in the model as confounding variables and previously generated explicit GM and WM masks were used, with a cluster extent threshold $k = 100$ voxels and significance level $p < 0.05$ after correction for multiple comparisons by controlling the family-wise error rate.

When significant between-group differences emerged at the voxel-based analyses, relationships between clinical variables (i.e., EDSS, SDMT, and motor scores) and MRI metrics (tissue probability, R1, and χ maps) were assessed voxel-wise via the TFCE toolbox using regression models with individual clinical scores as the dependent variables and explicit masks

restricting the analyses to areas of significant between-group differences. Robust partial correlation analyses, using bootstrap with 5000 resamples, were also carried out between clinical variables and global MRI metrics (i.e., T2-LL and tissue volumes and median R1 and χ values), correcting for age, sex, and TIV (for volumes only).

Results

Subjects

In total, 117 MS patients (85 relapsing-remitting, 22 secondary-progressive, 10 primary-progressive; 40.6 ± 11.9 years; F/M = 85/32) were included in the study, along with 53 HC (41.3 ± 11.6 years; F/M = 33/20) (Fig. 1). The mean disease duration (DD) for MS patients was 12.7 years (SD: 8.3), with a median EDSS score of 3.0 (interquartile range: 2.0–5.25) and a mean T2-LL of 6.2 ml (SD: 10.7). A total of 110 patients (94.0%) were under immunomodulatory treatment (32% with first-line therapies: interferon, glatiramer acetate, dimethyl fumarate, teriflunomide; 62% with second-line therapies: fingolimod, siponimod, natalizumab, alemtuzumab, ocrelizumab, cladribine) at the time of the MRI.

Demographic and clinical characteristics of the studied population, along with MRI-derived brain volumes and median R1 and χ values, are reported in Table 1.

Between-group comparisons

Compared to HC, MS patients had lower GM, WM, and whole-brain volume fractions (p -values ≤ 0.001 for all), along with lower median NAGM R1 ($p = 0.002$), NAWM R1, and χ ($p \leq 0.001$) values.

At the voxel-based analyses (Fig. 3 and Supplementary Table 1), MS patients showed massive clusters of reduced volume compared to HC, extensively encompassing both supra- and infra-tentorial GM and WM, with local maxima located in the bilateral thalami and fornices, respectively (p values < 0.001). Similarly, widespread clusters of reduced R1 values emerged in MS patients, extending well beyond the distribution of visible T2-hyperintense lesions and peaking in the corpus callosum, periventricular WM, and thalami (p values < 0.001). As for the analysis of QSM images, MS patients showed several clusters of reduced χ values compared to HC, involving the bilateral cerebral WM (particularly the frontal sections of the corpus callosum, corona radiata, superior longitudinal

Table 1 Demographic, clinical, and MRI characteristics of the studied population

	MS ($n = 117$)	HC ($n = 53$)	p value*** (MS vs HC)
Age (y)	40.6 ± 11.9	41.3 ± 11.6	0.71
Female sex*	85 (72.6%)	33 (62.3)	0.17
DMT (first line/second line/no therapy)*	38/72/7 (32.5/61.5/6.0%)	-	-
Disease Course (RR/SP/PP)*	85/22/10 (72.6/18.8/9.5%)	-	-
DD (y)	12.7 ± 8.3	-	-
EDSS**	3.0 (2.0 - 5.25)	-	-
Cognitive score	-0.82 ± 1.16	-	-
Motor score	-0.03 ± 0.86	-	-
T2-LL (ml)	6.2 ± 10.7	-	-
BPf (%)	78.3 ± 4.2	81.0 ± 2.9	< 0.001
GMf (%)	43.9 ± 2.8	45.3 ± 2.4	< 0.001
WMf (%)	34.4 ± 2.6	35.7 ± 2.0	< 0.001
NAGM median R1 (Hz)	0.66 ± 0.06	0.70 ± 0.06	0.002
NAWM median R1 (Hz)	0.99 ± 0.09	1.06 ± 0.09	< 0.001
NAGM median χ (ppb)	2.84 ± 1.81	2.44 ± 1.67	0.19
NAWM median χ (ppb)	-9.47 ± 2.58	-7.97 ± 2.31	< 0.001

Unless otherwise indicated, data are expressed as mean \pm SD. Between-group differences were tested with either Student t (age), Pearson Chi-square (sex), or age- and sex-corrected ANCOVA (MRI-derived measures) tests

*Data are the number of subjects, with percentages in parentheses

**Data are medians, with interquartile ranges in parentheses

***Significant between-group differences are reported in bold

DMT disease modifying treatment, RR relapsing-remitting, SP secondary-progressive, PP primary-progressive, EDSS Expanded Disability Status Scale, T2-LL T2 lesion load, BPf brain parenchymal fraction, GMf gray matter fraction, WMf white matter fraction, NAGM normal-appearing gray matter, NAWM normal-appearing white matter

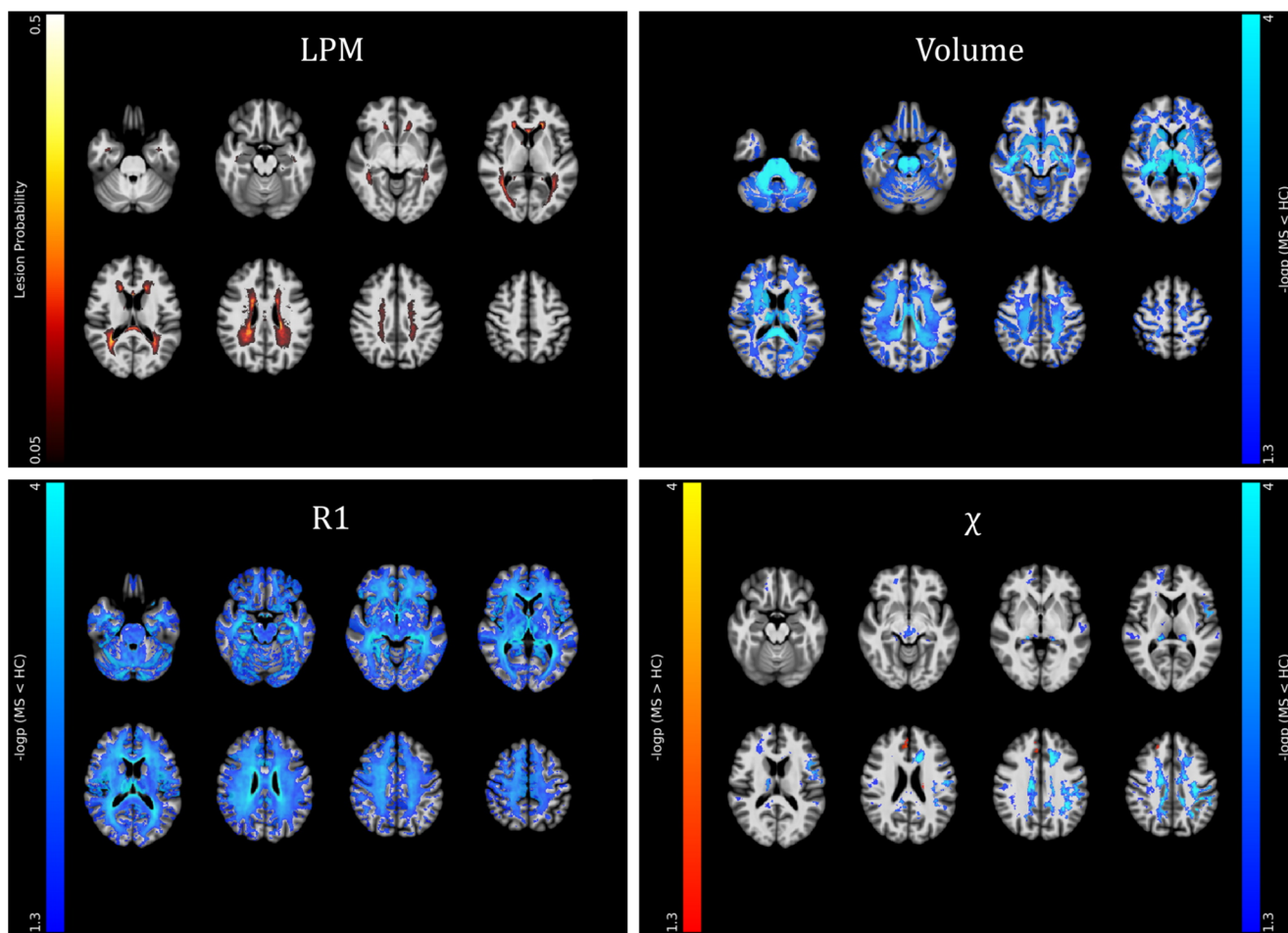


Fig. 3 Results of the between-group voxel-wise comparisons. A lesion probability map (LPM), obtained by summing all the binary lesion masks and dividing by the number of patients to give a lesion probability at each voxel, is presented (with a 5% probability threshold, upper left panel), along with clusters of significant between-group difference in terms of

volume (upper right panel), R1 and χ (lower panels) values for both the MS > HC (red-yellow) and MS < HC (blue-light blue) contrasts, all superimposed on axial sections of the average T1-weighted volume in the MNI space. For volume, R1, and χ maps, pooled results of the GM and WM analyses are shown. Images are in radiological orientation

fasciculus, and cingulum— p values < 0.001), the midbrain ($p = 0.001$) and the bilateral pulvinar and right thalamic ventral lateral nucleus (p -values < 0.001), along with small clusters of increased χ values in the left body of the caudate nucleus ($p = 0.004$), and the right anterior cingulate ($p = 0.005$) and superior frontal ($p = 0.02$) gyri.

Effect size (Cohen's d) maps of between-group differences in terms of regional volume, R1, and χ values (obtained from permutation-based T statistics estimated in the TFCE toolbox) are also presented in Fig. 4.

Relationship between MRI metrics and clinical status

When looking at the relationship with clinical variables, whole brain, and GM volumes were positively associated with motor performance ($r = 0.245$, $p = 0.009$ and $r = 0.241$, $p = 0.01$, respectively), with T2-LL and global GM volume correlating with cognitive processing speed ($r = -0.255$, $p = 0.006$ and $r = 0.234$, $p = 0.01$, respectively) and more weakly

with clinical disability ($r = 0.200$, $p = 0.03$ and $r = -0.203$, $p = 0.03$, respectively, not surviving multiple comparisons correction). No significant correlations emerged between clinical status and median R1 and χ values of both NAGM and NAWM (Table 2 and Supplementary Figure 2).

To allow for precise anatomical localization of the effects of interest, associations with clinical variables were also tested at the voxel level (Fig. 5 and Supplementary Table 2): thalamic volume was related both negatively with clinical disability ($p = 0.001$) and positively with cognitive processing speed ($p = 0.001$) and motor performance ($p = 0.01$), with additional positive correlations between the SDMT score and GM volume in the right basal ganglia and posterior insula (p values < 0.04) and between motor performance and infratentorial WM volume at the level of the medial lemnisci and cerebellar peduncles ($p = 0.01$). Furthermore, a large cluster of significant association between the SDMT score and R1 values emerged, extensively involving the (mainly posterior) periventricular WM and peaking around the right posterior

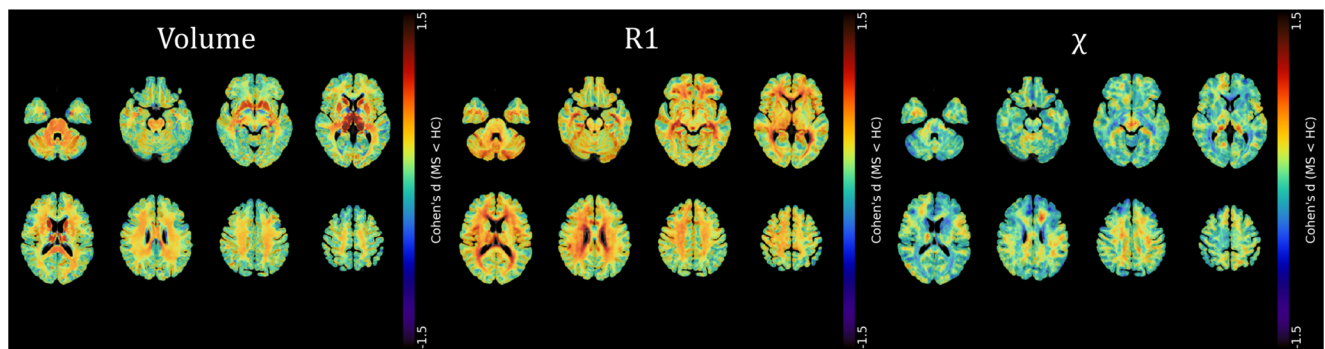


Fig. 4 Effect size maps of between-group differences. Effect size (Cohen’s *d*) maps of between-group differences in terms of volume, R1, and χ values (from left to right) are presented, superimposed on axial sections of the average T1-weighted volume in the MNI space. Positive

effect size values refer to the MS < HC contrast. For volume, R1, and χ maps, pooled results of the GM and WM analyses are shown. Images are in radiological orientation

thalamic radiation (*p* reaching 0.01), while χ values in the frontal sections of the cingulum and corona radiata were related both negatively with EDSS (*p* reaching < 0.001) and positively with motor performance (*p* reaching 0.003).

Discussion

Notwithstanding the many advances witnessed in the field of tissue microstructure in MS, none of the available MR techniques is solely affected by a specific pathological aspect, which advocates for the application of multi-parameter approaches to improve our understanding of microstructural damage [25, 31]. Here, we applied a multi-parameter analysis of volumetry and quantitative MRI to address the following questions: (i) what is the topography of iron and myelin changes assessed via susceptibility and relaxometry in MS? and (ii) are the observed changes clinically relevant?

As per the first question, MS patients showed a widespread R1 decrease across GM and WM regions, associated with substantially more limited modifications in susceptibility and with an atrophy pattern mainly involving deep GM, posterior and infratentorial regions. The observed R1 reduction throughout the WM was likely driven by changes in macromolecular tissue content (i.e., myelin), and, to a lesser extent, by iron levels [32]. Indeed, pathological descriptions documented demyelination not only in the context of lesions but also in normal-appearing WM [33], with iron depletion in remyelinated plaques [7] also possibly contributing, to a lesser extent, to R1 reduction. The R1 voxel-wise analysis confirms and expands previous findings reporting R1 decrease in multiple WM tracts in MS compared to HC [4], with no specific regional preference [34]. Similarly, the parallel susceptibility decrease in several WM regions confirms histopathological data reporting iron depletion in normal-appearing WM [7] and adds to a recent study reporting a decrease in susceptibility within the cingulum in a relatively small group of patients [35]. Indeed, our larger sample size and the

Table 2 Correlations between clinical and MRI-derived variables. Results are expressed as correlation coefficients (*r*) with 95% bias-corrected and accelerated bootstrap confidence intervals in parentheses (first row) and corresponding *p*-values (second row)

	EDSS	SDMT	Motor score
<i>Global MRI metrics^a</i>			
<i>T2-LL</i>	0.200 (0.033, 0.407) 0.03*	- 0.255 (- 0.360, - 0.151) 0.006	- 0.164 (- 0.324, - 0.029) 0.09
<i>Whole brain volume</i>	- 0.161 (- 0.356, 0.024) 0.09	0.177 (0.011, 0.339) 0.06	0.245 (0.078, 0.413) 0.009
<i>GM volume</i>	- 0.203 (- 0.370, - 0.027) 0.03*	0.234 (0.075, 0.386) 0.01	0.241 (0.089, 0.381) 0.01
<i>WM volume</i>	- 0.061 (- 0.246, 0.112) 0.52	0.057 (- 0.158, 0.257) 0.55	0.153 (- 0.016, 0.332) 0.11
<i>NAGM median R1</i>	- 0.136 (- 0.313, 0.053) 0.15	0.076 (- 0.094, 0.250) 0.42	0.039 (- 0.132, 0.210) 0.68
<i>NAWM median R1</i>	- 0.158 (- 0.331, 0.030) 0.10	0.167 (- 0.009, 0.338) 0.08	0.118 (- 0.042, 0.278) 0.22
<i>NAGM median χ</i>	0.007 (- 0.187, 0.196) 0.94	- 0.019 (- 0.201, 0.167) 0.84	- 0.022 (- 0.224, 0.193) 0.82
<i>NAWM median χ</i>	- 0.084 (- 0.291, 0.140) 0.38	- 0.030 (- 0.200, 0.141) 0.75	0.136 (- 0.049, 0.303) 0.15

Significant results are in bold

^a Correlations with clinical scores are corrected for age, sex, and TIV (for volumes only)

*Not significant after FDR correction

EDSS Expanded Disability Status Scale, SDMT Symbol Digit Modalities Test, *T2-LL* T2 lesion load, *GM* gray matter, *WM* = white matter, *NAGM* normal-appearing gray matter, *NAWM* normal-appearing white matter

application of a voxel-wise approach likely explain the increased sensitivity to the detection of between-group differences. Nevertheless, given previous histopathological data reporting a significant decrease of iron in oligodendrocytes and myelin within normal-appearing WM [7], the limited spatial extension of the observed susceptibility reduction is somehow surprising. A possible explanation could be that, as myelin and iron exert opposite effects on susceptibility, our ability to investigate tissues characterized by concomitant presence of demyelination and iron depletion remains intrinsically limited.

In GM, the observed R1 reduction was associated with decreased susceptibility in the thalamus and small clusters of increased susceptibility in the caudate nucleus and cortical areas. While R1 in the cortex and thalamus can be considered a reliable marker of myelin content [6, 36], in the basal ganglia it is highly influenced by iron concentration [6]. The observation that the thalamus undergoes structural modifications

similar to those observed in WM, with demyelination associated with iron depletion, confirms recent findings [6, 12, 37, 38] and can be explained by its peculiar anatomical structure. Likewise, our findings of small areas of increased susceptibility in the cortex and caudate nucleus are in line with recent reports, suggesting that susceptibility increase in MS deep GM, originally interpreted as demyelination and iron accrual [11, 12, 14], is mainly accounted for by atrophy rather than an actual increase in iron content [5, 6].

As per the clinical meaning of microstructural abnormalities, R1 changes seem to reflect the impact of focal lesions, with the cluster holding a significant correlation with cognitive performance peaking in the periventricular region, in overlap with focal demyelination, likely causing disconnection of distributed networks responsible for the control of high-level functions. On the other hand, susceptibility and atrophy, reflecting oligodendrocyte and axonal damage,

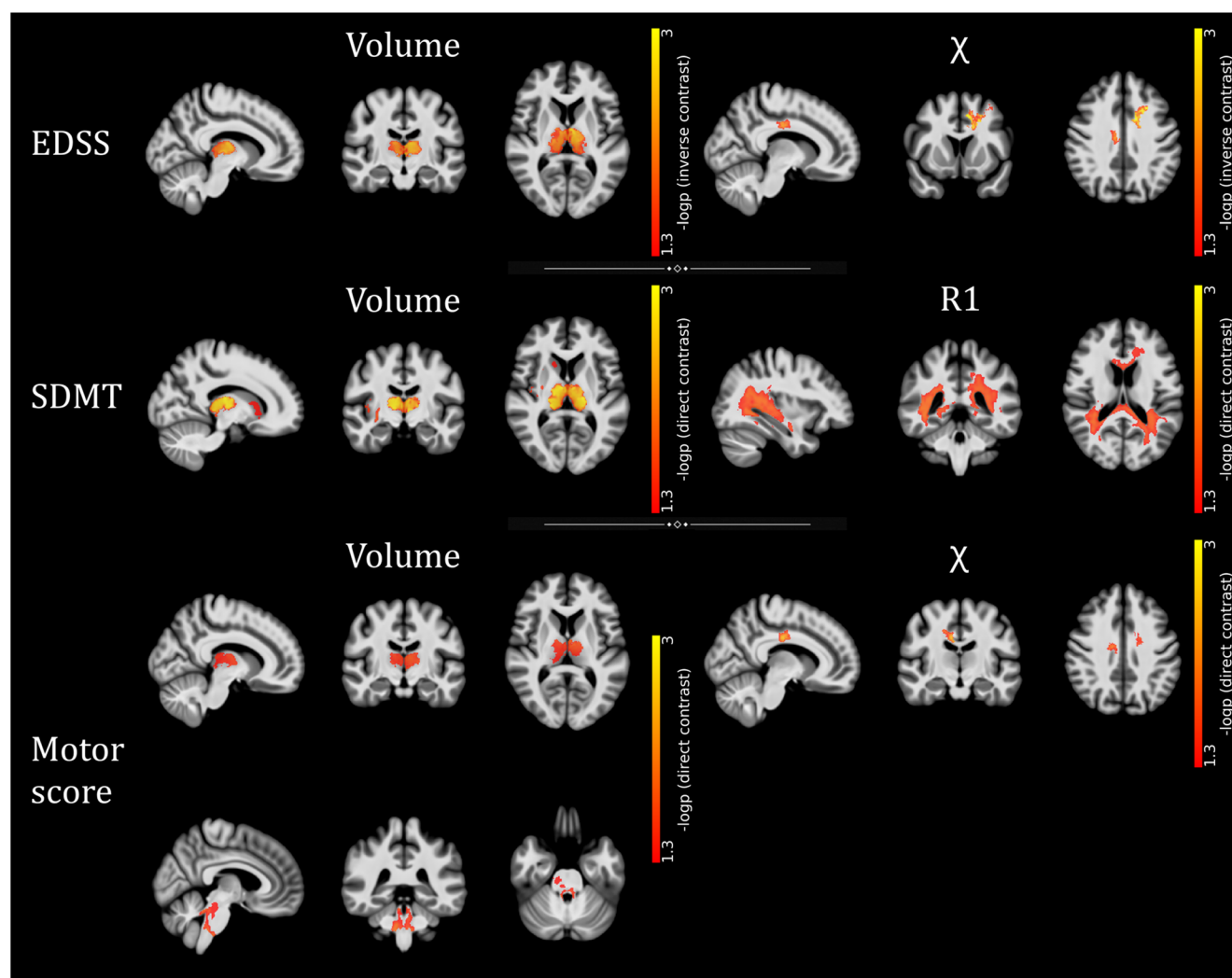


Fig. 5 Results of the voxel-wise correlations with clinical variables. Clusters of significant association between MRI metrics and EDSS, SDMT, and motor (from top to bottom) scores are presented,

superimposed on sagittal, coronal, and axial (from left to right) sections of the average T1-weighted volume in the MNI space. Images are in radiological orientation

significantly contributed to global and motor disability. Our analysis confirmed not only the central role of thalamic atrophy as a meaningful correlate of disability in MS [39] but also the relevance of cerebellar WM damage in driving motor impairment [40]. Beyond these confirmations, we identified a correlation between susceptibility reduction and disability that might add another layer to our understanding of the pathological mechanisms sustaining clinical impairment in MS. Indeed, if susceptibility decrease is the expression of oligodendrocyte damage [7], the consequent reduction of the tissue repair capability, depending upon oligodendrocyte activity, would contribute to the manifestation of clinical deficits. On the other hand, cognitive performance was related to deep GM atrophy and R1 abnormalities mostly overlapping the distribution of focal WM lesions. Such overlap, together with the correlation identified between lesion load and SDMT, suggests that, rather than microstructural damage, GM atrophy and disconnection sustained by focal lesions remain the main predictors of cognitive dysfunction in MS [41].

Our work is not without limitations. First, our assessment was conducted on the entire GM and WM rather than the normal-appearing tissue. However, when comparing extralésional median R1/susceptibility values at the group level, we identified significant differences, demonstrating that microstructural abnormalities also affect normal-appearing tissue. Additionally, the voxel-based analysis clearly demonstrated that such modifications are not spatially restricted to areas affected by T2 hyperintense lesions, as R1/susceptibility alterations are not only present where lesions have a higher probability to occur, but are also identified within normal-appearing tissue. Finally, although our clinical evaluation included motor and cognitive assessments, and our approach allowed for a multifaceted exploration of tissue abnormalities, we are still far from a comprehensive characterization of the structural substrate underpinning clinical disability in MS.

In conclusion, we confirmed the presence of widespread and clinically relevant demyelination, expressed by R1 decrease, and atrophy in MS. In addition, our findings suggest that also the more limited modifications of tissue susceptibility are clinically meaningful, possibly adding information on oligodendrocyte dysfunction and damage to the ones provided by demyelination and atrophy estimation.

Supplementary Information The online version contains supplementary material available at <https://doi.org/10.1007/s00330-022-09154-y>.

Funding Open access funding provided by Università degli Studi di Napoli Federico II within the CRUI-CARE Agreement. The authors state that this work has not received any funding.

Declarations

Guarantor The scientific guarantor of this publication is Giuseppe Pontillo, MD.

Conflict of interest The authors of this manuscript declare no relationships with any companies, whose products or services may be related to the subject matter of the article.

Statistics and biometry One of the authors has significant statistical expertise.

Informed consent Written informed consent was obtained from all subjects (patients) in this study.

Ethical approval Institutional Review Board approval was obtained.

Methodology

- prospective
- cross-sectional study
- performed at one institution

Open Access This article is licensed under a Creative Commons Attribution 4.0 International License, which permits use, sharing, adaptation, distribution and reproduction in any medium or format, as long as you give appropriate credit to the original author(s) and the source, provide a link to the Creative Commons licence, and indicate if changes were made. The images or other third party material in this article are included in the article's Creative Commons licence, unless indicated otherwise in a credit line to the material. If material is not included in the article's Creative Commons licence and your intended use is not permitted by statutory regulation or exceeds the permitted use, you will need to obtain permission directly from the copyright holder. To view a copy of this licence, visit <http://creativecommons.org/licenses/by/4.0/>.

References

1. Calabrese M, Magliozzi R, Ciccarelli O, Geurts JJ, Reynolds R, Martin R (2015) Exploring the origins of grey matter damage in multiple sclerosis. *Nat Rev Neurosci* 16:147–158
2. Does MD (2018) Inferring brain tissue composition and microstructure via MR relaxometry. *Neuroimage* 182:136–148
3. Stuber C, Pitt D, Wang Y (2016) Iron in multiple sclerosis and its noninvasive imaging with quantitative susceptibility mapping. *Int J Mol Sci* 17(1):100. <https://doi.org/10.3390/ijms17010100>
4. O'Muirheartaigh J, Vavasour I, Ljungberg E et al (2019) Quantitative neuroimaging measures of myelin in the healthy brain and in multiple sclerosis. *Hum Brain Mapp* 40:2104–2116
5. Schweser F, Hagemeyer J, Dwyer MG et al (2021) Decreasing brain iron in multiple sclerosis: The difference between concentration and content in iron MRI. *Hum Brain Mapp* 42:1463–1474
6. Pontillo G, Petracca M, Monti S et al (2021) Unraveling deep gray matter atrophy and iron and myelin changes in multiple sclerosis. *AJNR Am J Neuroradiol* 42:1223–1230
7. Hametner S, Wimmer I, Haider L, Pfeifenbring S, Bruck W, Lassmann H (2013) Iron and neurodegeneration in the multiple sclerosis brain. *Ann Neurol* 74:848–861
8. Hametner S, Endmayr V, Deistung A et al (2018) The influence of brain iron and myelin on magnetic susceptibility and effective transverse relaxation - a biochemical and histological validation study. *Neuroimage* 179:117–133
9. Mottershead JP, Schmierer K, Clemence M et al (2003) High field MRI correlates of myelin content and axonal density in multiple

- sclerosis—a post-mortem study of the spinal cord. *J Neurol* 250: 1293–1301
10. Schmierer K, Wheeler-Kingshott CAM, Tozer DJ et al (2008) Quantitative magnetic resonance of postmortem multiple sclerosis brain before and after fixation. *Magn Reson Med* 59:268–277
 11. Rudko DA, Solovey I, Gati JS, Kremenchutzky M, Menon RS (2014) Multiple sclerosis: improved identification of disease-relevant changes in gray and white matter by using susceptibility-based MR imaging. *Radiology* 272:851–864
 12. Zivadinov R, Tavazzi E, Bergsland N et al (2018) Brain iron at quantitative MRI is associated with disability in multiple sclerosis. *Radiology* 289:487–496
 13. Schmalbrock P, Prakash RS, Schirda B et al (2016) Basal ganglia iron in patients with multiple sclerosis measured with 7T quantitative susceptibility mapping correlates with inhibitory control. *AJNR Am J Neuroradiol* 37:439–446
 14. Fujiwara E, Kmech JA, Cobzas D et al (2017) Cognitive implications of deep gray matter iron in multiple sclerosis. *AJNR Am J Neuroradiol* 38:942–948
 15. Hernandez-Torres E, Wiggermann V, Machan L et al (2019) Increased mean R2* in the deep gray matter of multiple sclerosis patients: have we been measuring atrophy? *J Magn Reson Imaging* 50:201–208
 16. Polman CH, Reingold SC, Banwell B et al (2011) Diagnostic criteria for multiple sclerosis: 2010 revisions to the McDonald criteria. *Ann Neurol* 69:292–302
 17. Kurtzke JF (1983) Rating neurologic impairment in multiple sclerosis: an expanded disability status scale (EDSS). *Neurology* 33: 1444–1452
 18. Lublin FD (2014) New multiple sclerosis phenotypic classification. *Eur Neurol* 72(Suppl 1):1–5
 19. Goretti B, Nicolai C, Hakiki B et al (2014) The Brief International Cognitive Assessment for Multiple Sclerosis (BICAMS): normative values with gender, age and education corrections in the Italian population. *BMC Neurol* 14:171
 20. Fischer JS, Rudick RA, Cutter GR, Reingold SC (1999) The Multiple Sclerosis Functional Composite Measure (MSFC): an integrated approach to MS clinical outcome assessment. National MS Society Clinical Outcomes Assessment Task Force. *Mult Scler* 5: 244–250
 21. Monti S, Borrelli P, Tedeschi E, Coccozza S, Palma G (2017) RESUME: turning an SWI acquisition into a fast qMRI protocol. *PLoS One* 12:e0189933
 22. Palma G, Tedeschi E, Borrelli P et al (2015) A novel multiparametric approach to 3D quantitative MRI of the brain. *PLoS One* 10:e0134963
 23. Borrelli P, Palma G, Tedeschi E et al (2015) Improving signal-to-noise ratio in susceptibility weighted imaging: a novel multicomponent non-local approach. *PLoS One* 10:e0126835
 24. Borrelli P, Palma G, Comerci M, Alfano B (2014) Unbiased noise estimation and denoising in parallel magnetic resonance imaging 2014 IEEE International Conference on Acoustics, Speech and Signal Processing (ICASSP), pp 1230–1234
 25. Monti S, Pontillo G, Russo C, Cella L, Coccozza S, Palma G (2021) RESUME(N): a flexible class of multi-parameter qMRI protocols. *Phys Med* 88:23–36
 26. Ashburner J, Friston KJ (2000) Voxel-based morphometry—the methods. *Neuroimage* 11:805–821
 27. Draganski B, Ashburner J, Hutton C et al (2011) Regional specificity of MRI contrast parameter changes in normal ageing revealed by voxel-based quantification (VBQ). *Neuroimage* 55:1423–1434
 28. Smith SM, Nichols TE (2009) Threshold-free cluster enhancement: addressing problems of smoothing, threshold dependence and localisation in cluster inference. *Neuroimage* 44:83–98
 29. Field Andy P (2018) Discovering statistics using IBM SPSS statistics (5th ed.). SAGE Publications, London
 30. Winkler AM, Ridgway GR, Webster MA, Smith SM, Nichols TE (2014) Permutation inference for the general linear model. *Neuroimage* 92:381–397
 31. Inglese M, Petracca M (2018) MRI in multiple sclerosis: clinical and research update. *Curr Opin Neurol* 31:249–255
 32. Rooney WD, Johnson G, Li X et al (2007) Magnetic field and tissue dependencies of human brain longitudinal 1H2O relaxation in vivo. *Magn Reson Med* 57:308–318
 33. Allen IV, McKeown SR (1979) A histological, histochemical and biochemical study of the macroscopically normal white matter in multiple sclerosis. *J Neurol Sci* 41:81–91
 34. Vrenken H, Rombouts SA, Pouwels PJ, Barkhof F (2006) Voxel-based analysis of quantitative T1 maps demonstrates that multiple sclerosis acts throughout the normal-appearing white matter. *AJNR Am J Neuroradiol* 27:868–874
 35. Yu FF, Chiang FL, Stephens N et al (2019) Characterization of normal-appearing white matter in multiple sclerosis using quantitative susceptibility mapping in conjunction with diffusion tensor imaging. *Neuroradiology* 61:71–79
 36. Lutti A, Dick F, Sereno MI, Weiskopf N (2014) Using high-resolution quantitative mapping of R1 as an index of cortical myelination. *Neuroimage* 93(Pt 2):176–188
 37. Schweser F, Raffaini Duarte Martins AL, Hagemeyer J et al (2018) Mapping of thalamic magnetic susceptibility in multiple sclerosis indicates decreasing iron with disease duration: A proposed mechanistic relationship between inflammation and oligodendrocyte vitality. *Neuroimage* 167:438–452
 38. Pontillo G, Coccozza S, Lanzillo R et al (2019) Determinants of deep gray matter atrophy in multiple sclerosis: a multimodal MRI study. *AJNR Am J Neuroradiol* 40:99–106
 39. Eshaghi A, Prados F, Brownlee WJ et al (2018) Deep gray matter volume loss drives disability worsening in multiple sclerosis. *Ann Neurol* 83:210–222
 40. Coccozza S, Petracca M, Mormina E et al (2017) Cerebellar lobule atrophy and disability in progressive MS. *J Neurol Neurosurg Psychiatry* 88:1065–1072
 41. Benedict RHB, Amato MP, DeLuca J, Geurts JGG (2020) Cognitive impairment in multiple sclerosis: clinical management, MRI, and therapeutic avenues. *Lancet Neurol* 19:860–871

Publisher's note Springer Nature remains neutral with regard to jurisdictional claims in published maps and institutional affiliations.